

Spotted vesicles, striped micelles and Janus assemblies induced by ligand binding

David A. Christian^{1,2}, Aiwei Tian^{1,2,3}, Wouter G. Ellenbroek^{1,4}, Ilya Levental^{1,5}, Karthikan Rajagopal^{1,2}, Paul A. Janmey^{1,4,5}, Andrea J. Liu^{1,4}, Tobias Baumgart^{1,3,4} and Dennis E. Discher^{1,2,4,5*}

Selective binding of multivalent ligands within a mixture of polyvalent amphiphiles provides, in principle, a simple mechanism for driving domain formation in self-assemblies. Divalent cations are shown here to crossbridge polyanionic amphiphiles, which thereby demix from neutral amphiphiles and form spots or rafts within vesicles as well as stripes within cylindrical micelles. Calcium- and copper-crossbridged domains of synthetic block copolymers or natural lipid (phosphatidylinositol-4,5-bisphosphate) possess tunable sizes, shapes and/or spacings that can last for years. Lateral segregation in these 'ligand-responsive Janus assemblies' couples weakly to curvature and proves to be restricted within phase diagrams to narrow regimes of pH and cation concentration that are centred near the characteristic binding constants for polyacid interactions. Remixing at high pH is surprising, but a theory for strong lateral segregation shows that counterion entropy dominates electrostatic crossbridges, thus illustrating the insights gained into ligand-induced pattern formation within self-assemblies.

Amphiphiles of suitable proportions will self-assemble in water into vesicles as well as high-curvature micelles^{1–4}, and within such assemblies controlled demixing to form fully segregated 'Janus' assemblies has been postulated^{5–7}. Here, we show that divalent cations can drive mesoscale domain formation within assembled mixtures of neutral and anionic polymer amphiphiles, including both synthetic polymers and highly charged lipids. Ligand-responsive Janus assemblies that form only on addition of a ligand could allow new approaches to higher-order assemblies⁸, delivery of drugs⁹ and hierarchical patterning^{10,11}. So far, only nanoscale domains have been reported as present in block-copolymer mixtures, driven by fluorinated or crystallizing diblocks^{10,12,13}. For lipid bilayers, micrometre-sized domains have been documented, but domains have generally been induced by a mismatch of lipid acyl chains^{14–16}. Ion-induced domain formation in lipid vesicles is of interest in cell signalling and other dynamic membrane processes¹⁷, but past results obtained using lipids of net charge -1 or less seem highly controversial^{18,19}—possibly because lipid systems are soft and highly dynamic.

Charged block copolymers can generate morphologies that are stable but tunable after polymer synthesis by varying the pH and salt concentration^{4,20}. Polymer-based vesicular 'polymersomes' and worm-like micelles are mechanically tough compared with lipid assemblies, and polymers also provide broad choices in both chemistry and bilayer dimensions ($d \sim 10$ – 100 nm in Fig. 1a, inset) with properties tailored for insight and application^{1–4}. The stability of polymer assemblies generally increases with molecular weight M_n , exhibiting lifetimes ($\sim e^{M_n}$) that can reach years and that therefore permit equilibration. For mixtures of polyanionic and neutral amphiphiles, we hypothesized that cation crossbridging of the polyanions—including both block copolymers and some highly charged lipids—would be sufficiently strong to cause lateral segregation into stable mesoscopic 'gel' domains that would couple only weakly to curvature effects.

Spotted vesicles and calcium gelation

We initially studied mixtures of two polymer amphiphiles. A relatively symmetric poly(acrylic acid)–poly(butadiene) (PAA–PBD) copolymer denoted as AB1 ($M_n = 10,050$ g mol⁻¹, with hydrophilic fraction $f \approx 0.50$) yields polymersomes and micelles as a function of pH and salt concentration, whereas the non-ionic poly(ethylene oxide)–PBD (PEO–PBD) copolymer denoted as OB18 ($M_n = 10,400$ g mol⁻¹, $f \sim 0.35$) yields coexisting cylinders and vesicles independent of the pH and salt concentration. When OB18 is labelled with a rhodamine fluorophore (OB18*) and mixed with unlabelled AB1 in various proportions, calcium-induced domains or rafts can be clearly seen in almost all giant vesicles (Fig. 1a–c). Polymersomes were immobilized by aspiration into a micropipette, which not only facilitated z -stack imaging by laser scanning confocal microscopy but also established that the membranes are stable under applied tension. The result obtained from the analysis of the area fraction of AB1 domains corresponds closely to the copolymer blend ratio (see Supplementary Table S1); for example, 25% AB1 gave a total area fraction of 0.22 ± 0.10 ($n = 5$ vesicles). The low diffusivity of OB18 (ref. 1) minimizes drift effects that have frustrated similar high-resolution studies of lipid vesicles. Moreover, domains here could be observed for years after vesicle formation and yet domains also dissipate within minutes on addition of a calcium chelator (see Supplementary Fig. S1), indicating that calcium induces thermodynamically stable phase separation.

Strong lateral segregation (SLS) of the two copolymers was confirmed by simultaneous two-colour imaging of vesicles made with both OB18* and fluorescently labelled AB1 (denoted as AB1*) (Fig. 1d). Analysis of the fluorescence intensity of each colour for both phases shows a >3 -fold enrichment of OB18* in OB18-rich domains and a similar enrichment of AB1* in AB1-rich domains—although this is probably a minimum estimate that is limited by optics. The importance of calcium suggests that this divalent cation acts as a crossbridge between polyanionic AB1 chains and

¹Laboratory for Research on the Structure of Matter; ²Chemical & Biomolecular Engineering; ³ Chemistry; ⁴Physics & Astronomy; ⁵Bioengineering Graduate Groups, University of Pennsylvania, Philadelphia, Pennsylvania 19104, USA. *e-mail: discher@seas.upenn.edu.

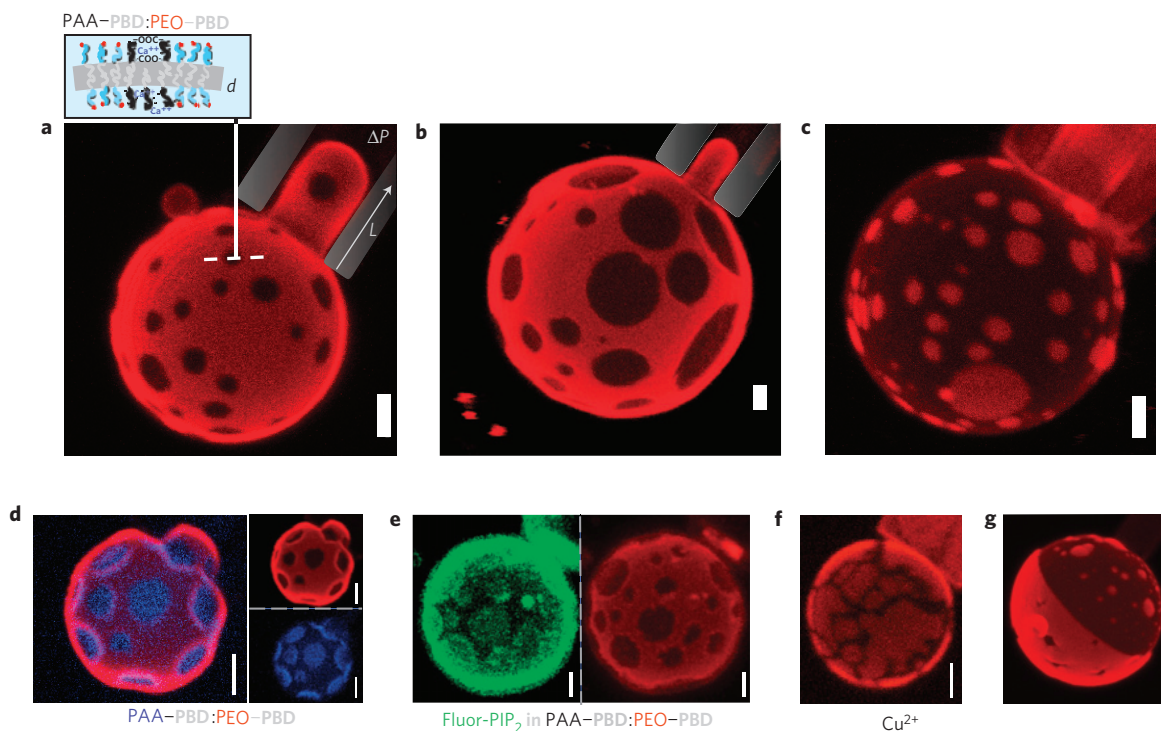


Figure 1 | Spotted vesicles imaged by z-sectioning confocal microscopy during aspiration in micropipettes. **a–c**, Cation-induced, lateral phase segregation of charged AB1 and neutral, fluorescently labelled OB18* diblock copolymers formed at pH₀ 4, 0.1 mM calcium at 25% (**a**), 50% (**b**) and 75% (**c**) AB1. The inset in **a** shows a schematic of a phase-separated membrane of thickness d . ΔP is the aspiration pressure in the micropipette, and L is the length of the aspirated projection. **d**, Two-colour micrograph of a phase-separated polymersome (34% AB1, AB1/AB1* = 10:1) with individual red (OB18*) and blue (AB1*) channel micrographs to illustrate the extent of demixing. **e**, Individual channels modified using an averaging smoothing filter to enhance the contrast for a two-colour phase-separated polymersome (50% AB1) with 2% PIP₂-BodipyFL (green) enriched in dark AB1 domains and partially segregated from the OB18*-rich domains (red). Unmodified images and fluorescence intensity analysis of domains are shown in Supplementary Fig. S2. **f**, Phase separation of AB1 (50%) induced by copper(II) at pH₀ 3.5, 0.075 mM copper(II). **g**, Janus polymersome resulting from domain coarsening in a 50% AB1 polymersome. Scale bars: 2 μm.

although the electrostatic basis for domain formation might seem intuitive, we show below that domain formation occurs only in a highly restricted regime of pH and ion concentration. To assess the possible generality of the effect, a highly anionic and fluorescently labelled lipid phosphatidylinositol-4,5-bisphosphate (PIP₂), was added to the polymer film; this, too was found enriched in the AB1-rich domains of vesicles (Fig. 1e). In a second test of the electrostatic interactions, another divalent cation, copper(II) transition metal, was added and indeed found to cause domain formation, although the domains appear more fractured (Fig. 1f, Supplementary Fig. S3), probably as a result of the stronger interactions between transition metals and PAA (refs 21, 22). The weaker crossbridging of AB1 by calcium apparently led to phase separation but not strong gelation, so it seems that AB1 molecules can diffuse to form circular domains that coarsen with time for minimizing boundary energy. Indeed, a hint of coarsening was seen in our initial studies with a few fully segregated ‘Janus’ vesicles having nearly homogeneous and distinct hemispheres (Fig. 1g).

To assess the coarsening and perhaps gain control over the domain size, we extended the hydration time. The results above were obtained by making polymersomes with overnight hydration of polymer films heated to 60 °C; longer hydration times did indeed give larger domains that coarsen until there is only ~1 domain per (15 μm² vesicle) after roughly 40 h (Fig. 2). The total area fraction of domains per vesicle remains constant at the initial mixing ratio, independently of the hydration time, indicating that the phase separation is always complete. Calcium-responsive Janus vesicles thus controllably form on timescales of days and prove stable for far longer.

In using micropipette aspiration to immobilize vesicles, we observed that the extent of aspirated membrane within the pipette depended on the phase being aspirated. Aspirated projections of the continuous OB18* phase (Fig. 1a,b) were seen at pressures of 70 Pa, whereas no significant projection could be obtained in the continuous AB1 phase (Fig. 1c) at pressures up to 500 Pa. The difference in domain deformability seemed consistent with an increase in membrane stiffness caused by calcium-mediated bridging between polyanionic chains. However, to study this in more detail, we aspirated pure AB1 polymer vesicles and determined an effective rigidity E_{app} for the membranes as a function of pH and calcium concentration²³. For gel networks²¹ or polymer brushes composed of weak polyelectrolytes such as PAA (ref. 22), increased ionization results in a greater calcium-bridging effect evident in gel or brush volume changes. Indeed, we find that at a constant calcium concentration of 0.1 mM (Fig. 3a), membrane rigidity increases 20-fold with ionization from E_{app} (pH₀ 4) \approx 0.6 mN m⁻¹ to E_{app} (pH₀ 6) \approx 12.7 mN m⁻¹, consistent with a 100-fold decrease in [H⁺] across the pK_a of PAA (pK_a \sim 5). The low-pH polymersomes also exhibit a spherical contour outside the pipette, typical of liquid-phase vesicles, whereas the stiffer, high-pH vesicles flatten near the pipette mouth as they buckle and distort, similar to covalently crosslinked solid polymersomes²³. Whether fluid-like or gel-like, these vesicles sustain membrane tensions and strains far above those achievable with lipid membranes. The stability is due to polymer membranes being several times thicker than lipid bilayers ($d \sim$ 4 nm) rather than being intrinsically stiffer.

With increasing pH, AB1 membranes become negatively charged, which promotes calcium bridging and membrane

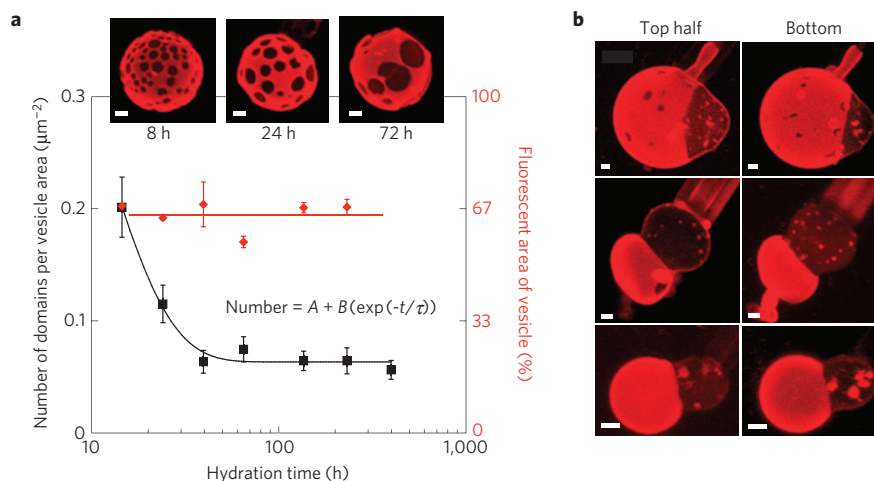


Figure 2 | Controlled coarsening yields Janus-like polymersomes. **a**, Mixed films of 33:67 AB1:OB18* were hydrated for the times indicated and vesicles were imaged at each time point (insets) to measure the domains per area (average \pm standard error, $n \geq 3$ per time point). The coarsening of domains is shown to saturate by ~ 40 h, but the '% area' occupied by domains remains relatively constant throughout. **b**, Most polymersomes showed fully segregated domains after two or more days. Scale bars: 2 μm .

rigidification (Fig. 3b). However, E_{app} is more sensitive to calcium concentration than to pH (Fig. 3c). The effective rigidity in either case is fitted to a power-law form:

$$E_{\text{app}} = A([\text{ion}]/K)^a \quad (1)$$

where [ion] is either $[\text{H}^+]$ or $[\text{Ca}^{2+}]$, K is the relevant dissociation constant, A is a prefactor and a is a power-law exponent. Best-fit parameters with equation (1) indicate stronger scaling for calcium than for protons ($a_{\text{Ca}} = 2.5$ versus $|a_{\text{H}^+}| = 0.34$). Calcium also gives much stronger scaling than the linear scaling of the polymer network rigidity that is expected with simple covalent crosslinkers; the enhancement indicates cooperative calcium interactions, perhaps by means of calcium-induced increases in brush ionization²². On the basis of these results, domains in the spotted polymersomes at low pH and only moderate $[\text{Ca}^{2+}]$ are likely to be liquid-like or weak gels—which is consistent with both circular domain shapes and also the noted resistance to aspiration.

The fluorescence recovery after photobleaching (FRAP) confirmed gelation in the 100% AB1 system. A cationic fluorescent dye (DiO-C18) mixed into the AB1 membranes allowed photobleaching of a small circular area (radius $\rho \sim 0.5 \mu\text{m}$) on top of individual vesicles and the time-dependent fluorescence recovery (Fig. 3d) gave characteristic diffusion times, τ_{D} , that proved small at very low pH but unmeasurably long at $\text{pH}_0 = 5$. The diffusivity $D = \rho^2/(4\tau_{\text{D}})$ for the cationic probe (Fig. 3e) is nearly linear with proton concentration in the transition regime ($\text{pH}_0 \sim 4$) even when fitted to a form similar to that for rigidity (equation (1)), that is, $D = B([\text{H}^+]/K)^b$ ($b \approx 0.9$ and $B = 9 \times 10^{-5} \mu\text{m}^2 \text{s}^{-1}$). FRAP studies with a neutral hydrophobic dye showed no diffusivity dependence on pH or calcium concentration, confirming that the gelation effects were confined to the PAA brush (see Supplementary Fig. S4). On the basis of the measured pH dependence of the membrane rigidity (Fig. 3b: $|a_{\text{H}^+}| = 0.34$), the ratio of mobility/rigidity exponents, $|b/a| \approx 2.5$, is seen to be much larger than that seen with dynamically crosslinked entanglements in bulk polymers, for which $|b/a| \approx 0.55$ (ref. 24). Electrostatic interactions are apparently more effective in slowing diffusion of AB1 chains than rigidifying the brush, whereas polymer entanglements have the opposite effect.

Striped cylinders

PAA at high pH becomes so highly charged that electrostatic repulsion in AB1 curves the core/brush interface and

generates cylindrical micelles²⁰. Mixtures with OB18* behave no differently—except for the narrow range of pH and calcium concentration in which cylinders appear striped (Fig. 4a). Image overlays clearly show that phase-separated cylinders are both continuous and flexible, with a persistence length of 5–10 μm , which is similar to that for pure systems²⁰.

Alternating dark and fluorescent segments are 0.3–1 μm in length and their area fractions are in approximate proportion to the blend ratios of AB1:OB18* (Fig. 4b; Supplementary Table S1). Striped nanoscale demixing with strongly segregating block copolymers has been predicted for small-diameter cylinders²⁵ and has been observed by electron microscopy both for fluoropolymer-based triblock copolymers¹⁰ and for semicrystalline diblocks in epitaxial growth of single nanostripes¹³. Here, calcium-mediated interactions yield periodic mesoscale domains that alternate in a periodic fashion that is correlated at length scales up to 17 μm (Fig. 4c, Supplementary Fig. S5). Distributions of fluorescent domain length L for all compositions fit well ($R^2 \geq 0.95$) to a linear growth model with termination by combination or coarsening, $P(L) \sim L \exp(2L/L_n)$ (Fig. 4d), giving a characteristic length L_n , that proves linear in copolymer ratio (Fig. 4d, inset; $R^2 = 0.96$) and that predicts tunable, ligand-dependent domain sizes from nanometres to micrometres. The uniformity in the width of the stripes could be due to the kinetics of domain formation. For example, if the AB1-rich domains have a lower spontaneous curvature than the OB18 domains, then phase separation might proceed by means of a periodic peristaltic mode²⁶. Coarsening of domains is unlikely in the quasi-one-dimensional geometry of a cylinder micelle, as there is little decrease in interfacial area with coarsening.

The phase diagram

Systematic mapping of the pH- and calcium-dependent phase diagram for the 25:75 copolymer mixture (Fig. 5a, Supplementary Fig. S6a) expands otherwise similar morphological studies with pure AB1 (ref. 20; shaded grey with AB1 morphology designated as spherical micelles, worm-like micelles and vesicles) and pinpoints a relatively narrow regime of SLS. From pH 3.5 to 5.5 and at $[\text{Ca}^{2+}] = 0.025$ to 0.4 mM, this stable window of SLS corresponds to chemical potential widths of just $\sim 2\text{--}5k_{\text{B}}T$ ($=k_{\text{B}}T \log n\{[\text{ion}]_{\text{max}}/[\text{ion}]_{\text{min}}\}$, where k_{B} is Boltzmann's constant). Spotted polymersomes dominate at intermediate pH and calcium level, but increases in pH and calcium destabilize the membranes and generate 'squids' of vesicle-connected cylinder micelles. Higher

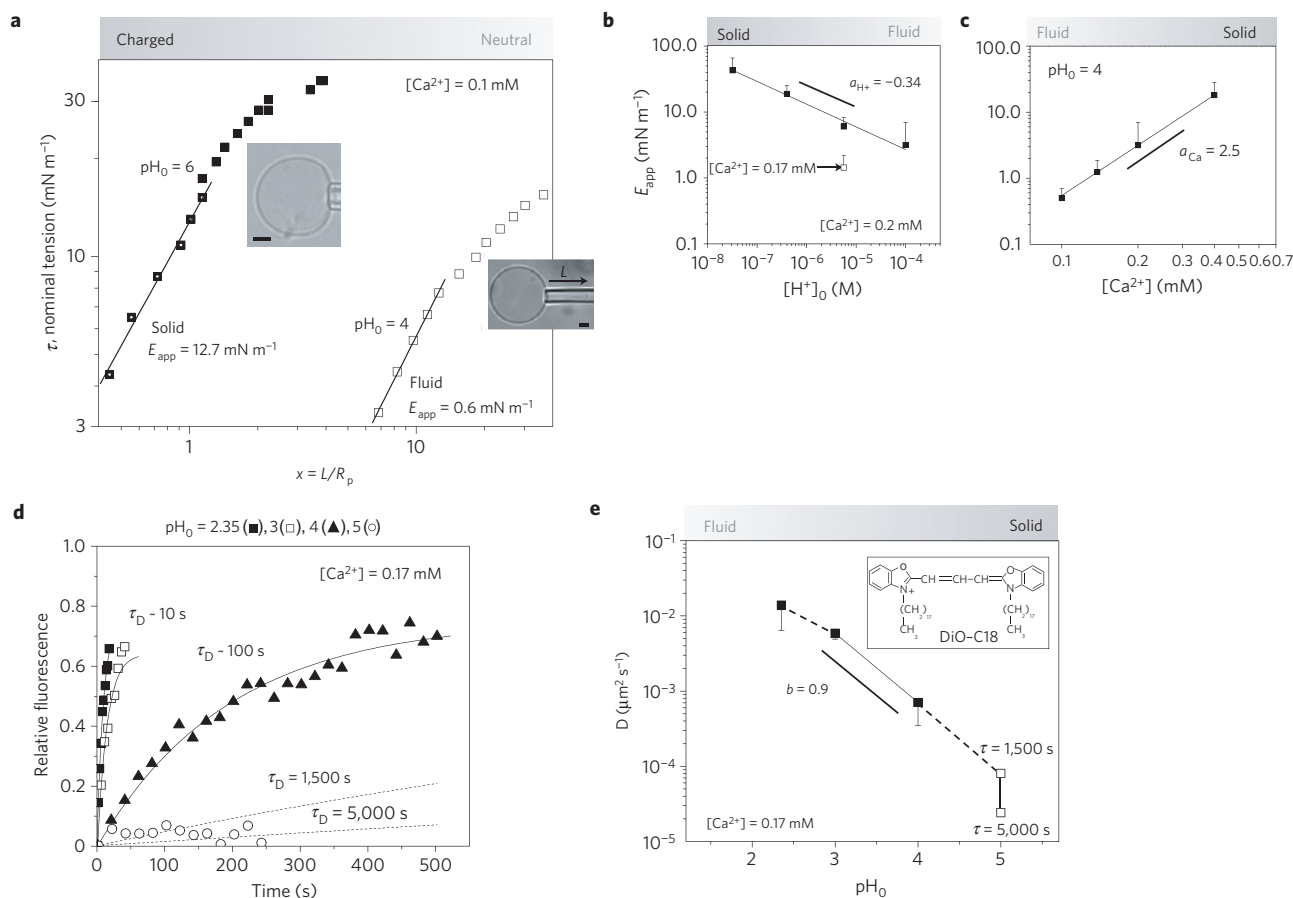


Figure 3 | Fluid-gel transition of a polyanionic polymersome brush with increasing pH or calcium concentration. **a**, Effective elasticity of AB1 polymersomes hydrated for the indicated Ca^{2+} concentration and pH_0 . Power-law fits for the low-strain regime provide a measure of effective rigidity $E_{\text{app}} = (\tau/x)^m$ in units of millinewtons per metre, revealing a fluid, elastic membrane at pH_0 4 ($m = 1$) and inelastic deformation of a gel-like membrane at pH_0 6 ($m = 1.25$). The inset images show spherical and non-spherical vesicle contours, consistent with fluid-like or solid-like behaviour, respectively (scale bars: $4 \mu\text{m}$). **b,c**, Power-law fits of E_{app} as a function of pH or calcium concentration quantify the stiffening and much stronger effects are found with calcium. Fitting with equation (1) yields the following. For $[\text{H}^+]$: $a_{\text{H}^+} = -0.34$, $A_{\text{H}^+} = 6.0 \text{ mN m}^{-1}$ using $\text{p}K_a = 5$ ($R^2 = 0.99$). For Ca^{2+} : $a_{\text{Ca}} = 2.5$ and $A_{\text{Ca}} = 0.002 \text{ mN m}^{-1}$ ($R^2 = 0.99$). **d,e**, Relative fluorescence intensity versus time from the FRAP of cationic DiO-C18 dye in AB1 polymersomes at varying pH_0 . The fits provide the characteristic diffusion times τ_D and the calculated diffusion coefficients versus pH_0 are fitted using a power law across the fluid-gel transition regime (solid line).

pH plus high calcium level leads, as predicted²⁷, to re-entrant micelles that are probably over-charged, with the result that their net charge is positive (see Supplementary Fig. S6b). As with pure AB1, the blend also shows a morphological vesicle-cylinder transition—striped cylinders rather than spotted polymersomes form by film rehydration—with a slight decrease in calcium level and an increase in pH. The fluid-to-gel transition of pure AB1 polymersomes (filled circles) and worm-like micelles (filled squares) is indicated by the blue (fluid) and orange (gel) points in the phase diagram. The dashed line provides an estimate of this transition, and clearly indicates that aqueous conditions must be permissive for AB1 gels to achieve phase separation in these assemblies.

The generality of the phase diagram was tested with initial studies of giant unilamellar vesicles (GUVs) containing fluorescent PIP_2 , which is amongst the most anionic of natural lipids (-4 charge near pH 7) and which is also a chief signalling lipid for the cytoplasmic leaflet of cell membranes²⁸. GUVs composed of 95% dioleoylphosphocholine, 4.9% PIP_2 and 0.1% BodipyTR- PIP_2 and formed by electroformation at 37°C appeared homogeneous at pH 7.5 (see Supplementary Fig. S7a). The addition of lipid GUVs to calcium-containing buffer ($[\text{Ca}^{2+}] = 500 \mu\text{M}$) induced domains enriched in PIP_2 within minutes (see Supplementary Fig. S7b). Domain formation was reversed with the addition of a

calcium chelator (see Supplementary Fig. S7c). GUVs incubated in pH = 3 buffer (where PIP_2 has a net charge near -1) appeared homogeneous (see Supplementary Fig. S7d) and no domains were visible in GUVs incubated at pH = 3, $[\text{Ca}^{2+}] = 500 \mu\text{M}$ (see Supplementary Fig. S7e). These lipid results show that calcium induces phase separation in mixed lipid vesicles as well as in mixed polymer vesicles and also emphasize that SLS occurs only in a narrow region in pH.

Strong lateral segregation theory

A simple equilibrium model for SLS was derived on the basis of calcium-mediated attraction between polyanionic chains. Although attractions, or crossbridges, lead to gelation (above the blue dashed line in Fig. 5a), a mixture of competing effects restrict calcium-mediated lateral segregation to an even narrower window of calcium concentration and pH. A high net charge favours mixing, as electrostatic repulsion is high in domains rich in polyanions. As a result, SLS does not occur at low $[\text{Ca}^{2+}]$, where there is little counterion condensation and the net charge of the aggregates is highly negative. The same effect prevents segregation at high $[\text{Ca}^{2+}]$, where the charge apparently inverts to a high net positive charge on the aggregates. At high $[\text{H}^+]$ ($\text{pH} < \text{p}K_a$ for PAA), few charged groups on the AB1 chains condense the Ca^{2+} required

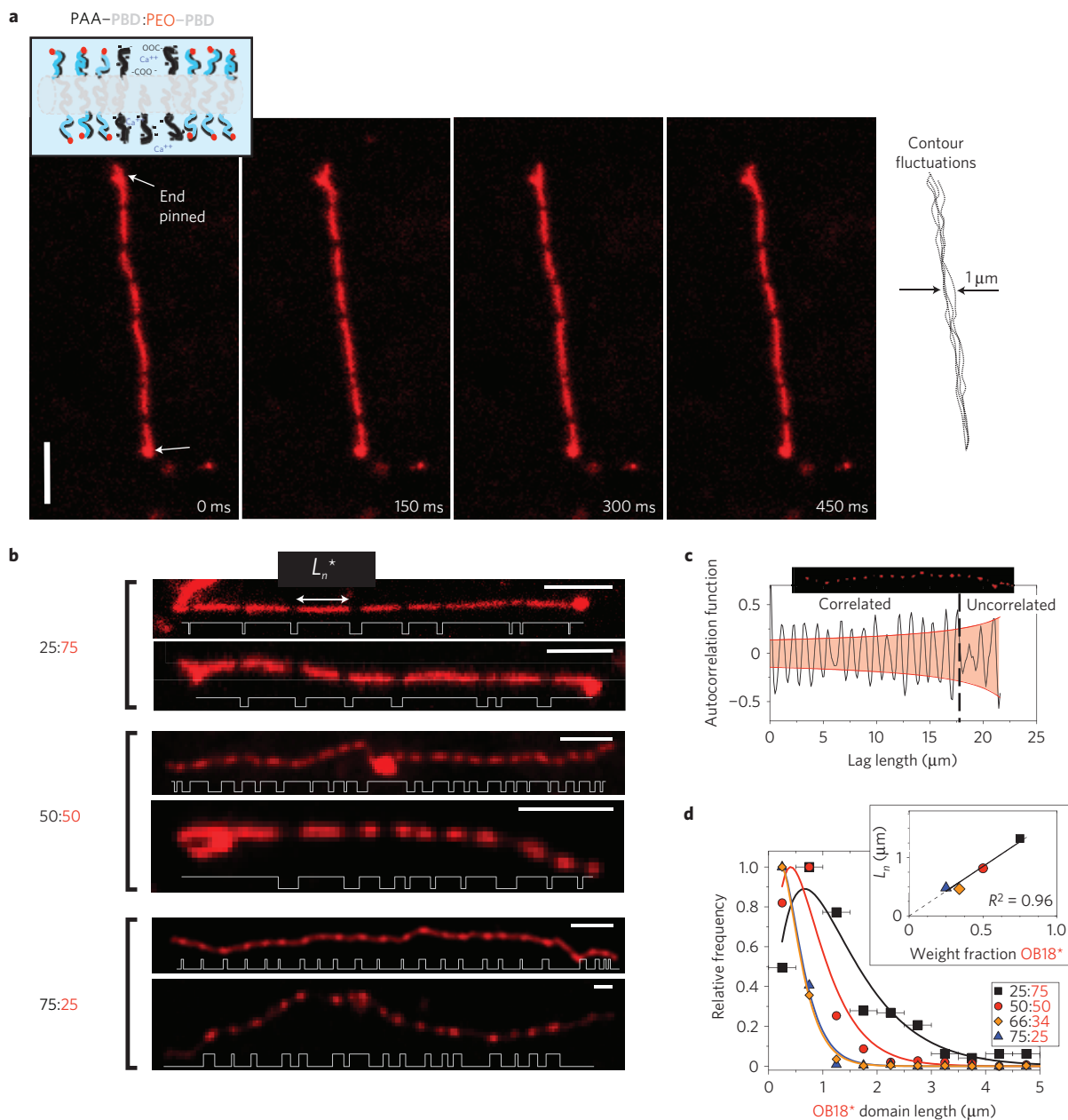


Figure 4 | Striped cylinder micelles. **a**, Time sequence of a pinned, striped worm-like cylinder micelle formed with AB1:OB18* = 25:75 at pH₀ 4.5 and [Ca²⁺] = 0.05 mM; the micelle remains flexible, as is evident in the contour overlay. **b**, Striped cylinder micelles formed at increasing AB1 fraction, although for any sample only about 10% of cylinders appeared definitively striped with multiple micrometre-sized bands. Plots of thresholded fluorescence intensity along the worm contour length highlight average domain size and periodicity. **c**, The long-range ordering of a single 75:25 worm micelle is at least 17 μm , as determined by examining the autocorrelation of the backbone fluorescence intensity. **d**, Domain lengths (L) of OB18* in striped cylinders at varying AB1 fraction are fitted to a Zimm-Schulz model ($R^2 \geq 0.95$) in which the number average length, L_n^* , scales linearly ($R^2 = 0.96$) with the OB18* blend fraction (inset). The error bars represent bin sizes for L . Scale bar: 4 μm .

to form crossbridges and therefore mixing between the nearly neutral AB1 and neutral OB18 is observed. As [H⁺] decreases, the system segregates with increasing crossbridging, but at lower [H⁺], the entropic penalty associated with confining condensed Ca²⁺ in PAA-rich domains increases, favouring mixing once again.

The free energy of the polymer-counterion system is calculated as a function of [H⁺], [Ca²⁺] and ϕ_A , the local fraction of AB1 chains. The role of proton concentration is approximated as setting the 'bare' charge of the AB1, using standard acid dissociation with a $\text{p}K_a \sim 5$. Assuming either cylindrical or bilayer geometry, the ion concentrations in the hydrophilic brush of the assembly, [H⁺]_b and [Ca²⁺]_b, are calculated using Oosawa's two-state approach to

counterion condensation²⁹ including electrostatic screening. The counterion entropy density s is given by

$$s \approx [\text{H}^+]_b \log_n [\text{H}^+]_b + [\text{Ca}^{2+}]_b \log_n [\text{Ca}^{2+}]_b \quad (2)$$

In a full electrostatic treatment, Ca²⁺ crossbridges would arise naturally from counterion correlations beyond counterion condensation. Here, we treat them phenomenologically, such that the effective attraction energy per crossbridge, E_c , is a fitting parameter and the number of crossbridges is estimated by interpolating between two expected limiting behaviours. We assume that every Ca²⁺ ion in the brush is close to a charged acrylic acid group.

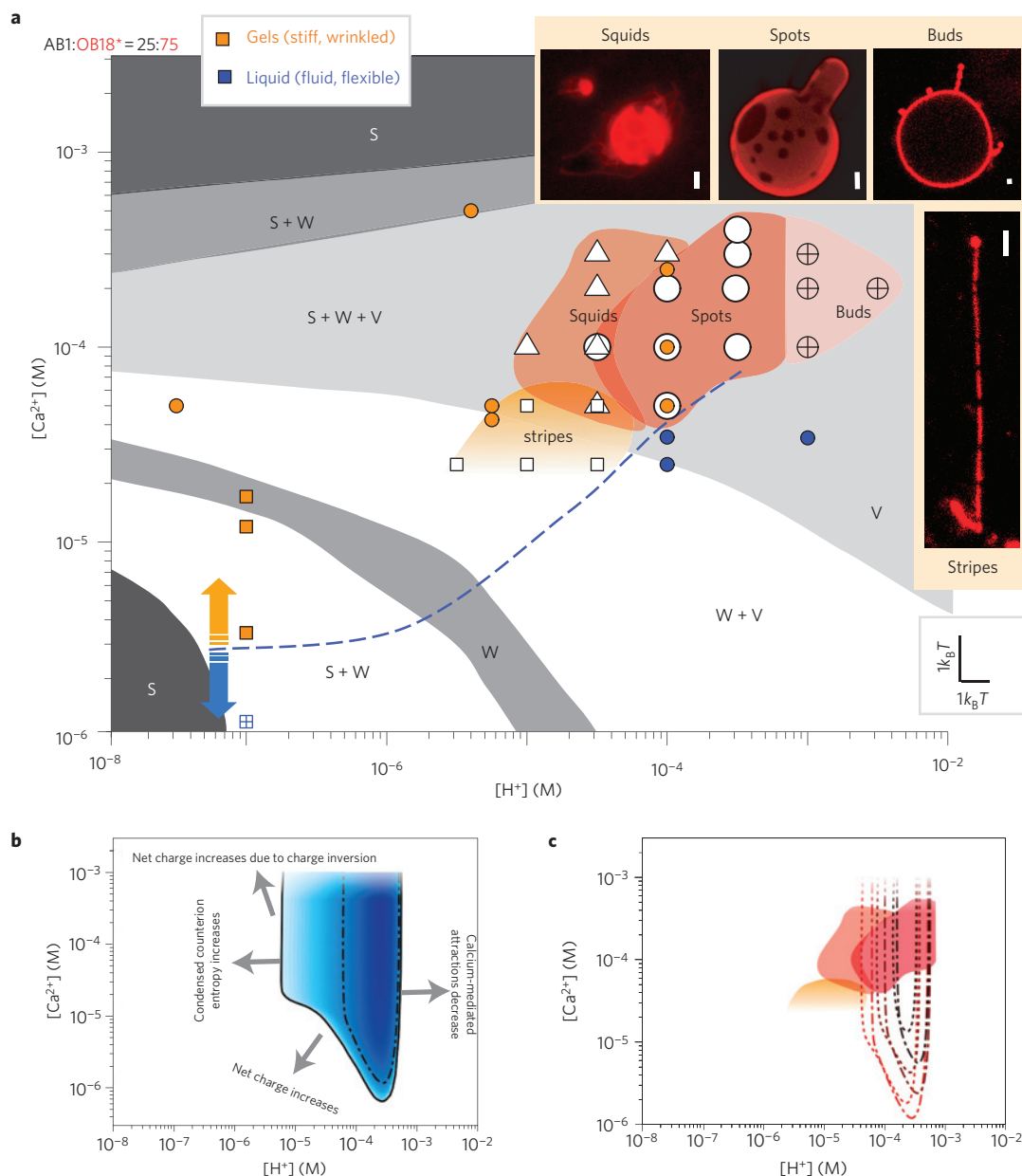


Figure 5 | Phase diagram with a narrow regime of domain formation for AB1:OB18* = 25:75 as observed experimentally and modelled theoretically.

a, A systematic experimental phase diagram of domain formation for 25% AB1 is overlaid on the morphological phase diagram for pure AB1 (shown in grey; spherical micelles (S), worm-like micelles (W) and vesicles (V)) and shown with points where experiments indicate whether pure AB1 polymersomes (coloured circles) and worm-like cylinder micelles (coloured squares) show fluid (blue) or gel (orange) characteristics. The calcium values in the morphological phase diagram were recalculated to correspond to the 0.025 mg ml^{-1} AB1 present in the blends used for domain formation and pH was converted to $[\text{H}^+]$. Four regions of interest were observed—squids, spots, buds and stripes—as shown in the inset images (scale bar: $2 \mu\text{m}$). **b**, The narrow window of domain formation observed experimentally is reproduced using a theoretical model (solid line). Increasing blue intensity in the region of domain formation is indicative of increasing contrast between laterally segregated domains, where the dashed-dotted line bounds the region where the contrast is larger than 50%. The dominating physical mechanisms for mixing are indicated with text. **c**, Contours for 50% contrast are plotted for other constituent ratios where increasing line thickness represents an increase in AB1 fraction (25, 50, 75%) for cylinder micelles (dotted lines) and polymersomes (dashed-dotted lines). These contours are plotted over the region of experimentally observed domain formation. The high calcium boundary is not obtained because the theoretical model does not capture charge inversion.

A crossbridge then forms when a Ca^{2+} ion is also close to a second charged acrylic acid group in a second AB1 molecule. In regions of low ϕ_A (and hence low $[\text{Ca}^{2+}]$), this process is limited by the lateral fluctuations of the PAA chains and the crossbridge density is $n_{c,\text{small}} = \sigma[\text{AA}^-][\text{Ca}^{2+}]$. The prefactor σ depends on the chain lengths and brush density. If all densities are expressed in ‘per polymer chain’ units then $\sigma = 0.83$, but our result is robust against variations of this parameter. At moderately large ϕ_A , the

crossbridge density is limited by the available Ca^{2+} ions and is therefore $n_{c,\text{large}} = [\text{Ca}^{2+}]$. We interpolate between the two limits by using $n_c = (n_{c,\text{small}}^{-3} + n_{c,\text{large}}^{-3})^{-1/3}$. The free energy includes a term for electrostatic self-energy and a Flory–Huggins-like term for the polymer chains as well as the counterion entropy (equation (2)). We determine the phase behaviour using a double-tangent construction in ϕ_A ; the region in which phase separation occurs is enclosed by a solid black line in Fig. 5b for $E_c = 6k_B T$ for vesicles with an AB1

fraction of 25%. The darkness within this region corresponds to the magnitude of a contrast function (0 when mixed, 1 when separated into domains of $\phi_A = 0$ and $\phi_A = 1$) and the dashed-dotted line corresponds to the contour with a contrast of 0.5. Such contours are plotted for worms (dotted) and vesicles (dashed-dotted) at AB1 fractions of 25, 50 and 75% (Fig. 5c). These contours are superimposed on the experimental region of SLS. Note that this simple model cannot capture the charge inversion of the aggregates, which is a counterion correlation effect and therefore cannot reproduce the high- $[\text{Ca}^{2+}]$ end of the phase diagram correctly. The model also predicts phase separation at $[\text{Ca}^{2+}]$ significantly lower than observed experimentally. This result is not unexpected, as phenomenological treatment of the electrostatics does not yet account for the cooperative interaction between calcium and PAA that was demonstrated here by rigidity measurements in which $a_{\text{Ca}}/a_{\text{H}^+} \approx 7$ (Fig. 3b) exceeds the simple doubling expected from charge differences between Ca^{2+} and H^+ . However, close to the line of zero net charge, the present model reproduces the finite region of phase separation as observed in experiment.

Spotted polymersomes that were induced here by ligand binding constitute responsive Janus structures that are highly tunable and stable even at nearly physiological conditions (see Supplementary Fig. S8). SLS is observed only within a narrow window of solution conditions but in structures as diverse as polymer vesicles, lipid vesicles and polymer cylinder micelles. The results indicate that the phenomenon is electrostatic in origin and can therefore occur in a wide range of systems: domain shape should be influenced by the addition of different metal cations (thus far copper and calcium but not sodium) or chelating agents (for example, EDTA) and domain formation should also occur with polybasic amphiphiles—although the limited biological application of positively charged assemblies (because they bind non-specifically to all negatively charged cell membranes and extracellular matrix) motivates further study of more polyanionic assemblies with physiological cations such as calcium. The results here thus open new routes to dynamic control over structural organization and functionalization within self-assembled synthetic materials.

Methods

Block copolymers PEO₈₀-PBD₁₂₅ ($M_n = 10,400 \text{ g mol}^{-1}$, polydispersity PD = 1.1, designated OB18) or PAA₇₅-PBD₁₀₃ ($M_n = 10,050 \text{ g mol}^{-1}$, PD = 1.1, designated AB1) were synthesized by standard polymerization and used as described²⁰. Lipids were purchased from either Avanti Polar Lipids (dioleoylphosphocholine, PIP₂) or Echelon Biosciences (BodipyFL-PIP₂, BodipyTR-PIP₂). The fluorophores tetramethyl rhodamine-5 carbonyl azide (TMRCa) and cascade blue ethylenediamine were purchased from Molecular Probes. Domain formation in polymersomes and worm-like micelles was observed by dissolving fluorescently labelled OB18 (OB18*) and AB1 polymers in chloroform and methanol and then drying to form a blended polymer film. The films were then hydrated in aqueous solution with known pH and calcium concentrations tuned by the addition of HCl and CaCl₂. OB18* was made by attaching TMRCa to the hydroxyl end group of the PEO block. The modification involves TMRCa conversion to an isocyanate, which then modified the hydroxyl end group of PEO to a urethane. This modification of the end group was carried out in toluene at 80 °C for 12 h. Excess, unreacted TMRCa dye was removed by a recrystallization and washing process with methanol, as verified by gel permeation chromatography. AB1* was made by attaching the amine-containing cascade blue to acrylic acid monomers along the backbone of the PAA chain using standard carbodiimide chemistry. Cascade blue was added in three-times excess of AB1 polymer and unreacted dye was removed by dialysis and washes with water and methanol. Fluorescence microscopy and micropipette aspiration were carried out as previously described^{15,25} (see Supplementary Methods for further details).

Received 26 January 2009; accepted 14 July 2009;
published online 6 September 2009

References

- Discher, D. E. & Eisenberg, A. Polymer vesicles. *Science* **297**, 967–973 (2002).
- Pochan, D. J. *et al.* Toroidal triblock copolymer assemblies. *Science* **306**, 94–97 (2004).
- Won, Y. Y., Davis, H. T. & Bates, F. S. Giant wormlike rubber micelles. *Science* **283**, 960–963 (1999).

- Zhang, L. F., Yu, K. & Eisenberg, A. Ion-induced morphological changes in ‘crew-cut’ aggregates of amphiphilic block copolymers. *Science* **272**, 1777–1779 (1996).
- Fraaije, J., van Sluis, C. A., Kros, A., Zvelindovsky, A. V. & Sevink, G. J. A. Design of chimaeric polymersomes. *Faraday Discuss.* **128**, 355–361 (2005).
- Srinivas, G. & Pitera, J. W. Soft patchy nanoparticles from solution-phase self-assembly of binary diblock copolymers. *Nano Lett.* **8**, 611–618 (2008).
- Walther, A. & Muller, A. H. E. Janus particles. *Soft Matter* **4**, 663–668 (2008).
- Glotzer, S. C. & Solomon, M. J. Anisotropy of building blocks and their assembly into complex structures. *Nature Mater.* **6**, 557–562 (2007).
- Alexeev, A., Uspal, W. E. & Balazs, A. C. Harnessing Janus nanoparticles to create controllable pores in membranes. *ACS Nano* **2**, 1117–1122 (2008).
- Cui, H. G., Chen, Z. Y., Zhong, S., Wooley, K. L. & Pochan, D. J. Block copolymer assembly via kinetic control. *Science* **317**, 647–650 (2007).
- Wang, H., Wang, X. S., Winnik, M. A. & Manners, I. Redox-mediated synthesis and encapsulation of inorganic nanoparticles in shell-cross-linked cylindrical polyferrocenylsilane block copolymer micelles. *J. Am. Chem. Soc.* **130**, 12921–12930 (2008).
- Li, Z. B., Kesselman, E., Talmon, Y., Hillmyer, M. A. & Lodge, T. P. Multicompartment micelles from ABC miktoarm stars in water. *Science* **306**, 98–101 (2004).
- Wang, X. S. *et al.* Cylindrical block copolymer micelles and co-micelles of controlled length and architecture. *Science* **317**, 644–647 (2007).
- Baumgart, T., Hess, S. T. & Webb, W. W. Imaging coexisting fluid domains in biomembrane models coupling curvature and line tension. *Nature* **425**, 821–824 (2003).
- Korlach, J., Schwille, P., Webb, W. W. & Feigenson, G. W. Characterization of lipid bilayer phases by confocal microscopy and fluorescence correlation spectroscopy. *Proc. Natl Acad. Sci. USA* **96**, 8461–8466 (1999).
- Veatch, S. L. & Keller, S. L. Separation of liquid phases in giant vesicles of ternary mixtures of phospholipids and cholesterol. *Biophys. J.* **85**, 3074–3083 (2003).
- Clapham, D. E. Calcium signalling. *Cell* **131**, 1047–1058 (2007).
- Haverstick, D. M. & Glaser, M. Visualization of Ca^{2+} -induced phospholipid domains. *Proc. Natl Acad. Sci. USA* **84**, 4475–4479 (1987).
- Shoemaker, S. D. & Vanderlick, T. K. Calcium modulates the mechanical properties of anionic phospholipid membranes. *J. Colloid Interface Sci.* **266**, 314–321 (2003).
- Geng, Y., Ahmed, F., Bhasin, N. & Discher, D. E. Visualizing worm micelle dynamics and phase transitions of a charged diblock copolymer in water. *J. Phys. Chem. B* **109**, 3772–3779 (2005).
- Horkay, F., Tasaki, I. & Bassar, P. J. Effect of monovalent–divalent cation exchange on the swelling of polyacrylate hydrogels in physiological salt solutions. *Biomacromolecules* **2**, 195–199 (2001).
- Konradi, R. & Ruhe, J. Interaction of poly(methacrylic acid) brushes with metal ions: Swelling properties. *Macromolecules* **38**, 4345–4354 (2005).
- Discher, B. M. *et al.* Cross-linked polymersome membranes: Vesicles with broadly adjustable properties. *J. Phys. Chem. B* **106**, 2848–2854 (2002).
- Gell, C. B., Graessley, W. W. & Fetters, L. J. Viscoelasticity and self-diffusion in melts of entangled linear polymers. *J. Polym. Sci. B* **35**, 1933–1942 (1997).
- Velichko, Y. S. & de la Cruz, M. O. Pattern formation on the surface of cationic–anionic cylindrical aggregates. *Phys. Rev. E* **72**, 041920 (2005).
- Grason, G. M. & Santangelo, C. D. Undulated cylinders of charged diblock copolymers. *Eur. Phys. J. E* **20**, 335–346 (2006).
- Borisov, O. V. & Zhulina, E. B. Reentrant morphological transitions in copolymer micelles with pH-sensitive corona. *Langmuir* **21**, 3229–3231 (2005).
- McLaughlin, S. & Murray, D. Plasma membrane phosphoinositide organization by protein electrostatics. *Nature* **438**, 605–611 (2005).
- Oosawa, F. *Polyelectrolytes* (M. Dekker, 1971).

Acknowledgements

The NSF-MRSEC at the University of Pennsylvania provided primary support. Further support from the NIH (D.E.D., P.A.J.), DOE (A.J.L.) and NSF (T.B.) is very gratefully acknowledged. We thank J. D. Pajeroski for his help with correlation length and periodicity analysis.

Author contributions

D.A.C., A.T., I.L., P.A.J., T.B. and D.E.D. designed experiments and analysed data; D.A.C., A.T. and I.L. carried out experiments; W.G.E. and A.J.L. developed the SSL theory; K.R. contributed new reagents; D.A.C., W.G.E., A.J.L., T.B. and D.E.D. wrote the paper.

Additional information

Supplementary information accompanies this paper on www.nature.com/naturematerials. Reprints and permissions information is available online at <http://npg.nature.com/reprintsandpermissions>. Correspondence and requests for materials should be addressed to D.E.D.